

From quark-gluon plasma to hadron spectra

P.V. Ruuskanen^a

^aDepartment of Physics, University of Jyväskylä,
P.O. Box 35, FIN-40351 Jyväskylä, Finland

Results on initial transverse energy production based on NLO perturbative QCD calculation with final state saturation of produced minijets are used to fix the initial energy density of produced matter. Assuming rapid thermalization, this provides the initial conditions for a hydrodynamic description of the expansion of final matter. Given a prescription of the decoupling of particles from the thermal system to free particles, final transverse spectra of hadrons and integrated quantities like multiplicity and transverse energy can be calculated in the central rapidity region. Results are reported and compared with measurements.

1. INTRODUCTION

Conservative estimates from the measured transverse energy and particle multiplicity at RHIC indicate that energy and particle densities well above those of normal nuclear matter are formed in nuclear collisions. Results from perturbative QCD (pQCD) calculation of minijet production with final state saturation [1] follow well the measured multiplicities. However, the calculated transverse energy per unit (pseudo)rapidity is larger by a factor ~ 2.6 than the measured value. For achieving agreement between the calculation and the experiment, the evolution of the produced matter must transfer a large fraction of the energy from mid-rapidity towards the fragmentation regions. In the hydrodynamic description the mechanism for the energy transfer is the work done by the pressure in the expansion. Assuming that initially the expansion is mainly in the longitudinal direction leads to an asymmetry between the transverse and longitudinal directions and to the desired energy transfer.

The work and the cooling of the matter during expansion will change the momentum distributions both in transverse and the longitudinal direction. In this work we assume that in the mid-rapidities the longitudinal flow follows the scaling law, $v_z = z/t$ (collision takes place at $t = 0$ and $z = 0$) and that we can ignore the small longitudinal changes of densities. With these restricting assumptions we are not able to address the problem of longitudinal momentum distributions but we can calculate the final transverse momentum distributions when the particles decouple at the end of the thermal stage. Calculation of spectra, the folding of flow with thermal motion, is performed using the Cooper and Fry [2] prescription.

The justification for the use of hydrodynamics can be marginal for some parts of the produced system but, first, it is clear that the bulk of the matter is very dense leading to

numerous secondary collisions and, second, in describing the energy-momentum transfer due to these collisions in terms of hydrodynamics the conservation laws are correctly satisfied.

2. INITIAL CONDITIONS FROM pQCD MINIJETS

The perturbative QCD calculation of minijet production is a momentum space calculation. In order to define the initial densities a connection between the momentum of the minijet and its space-time formation point is needed. At collider energies the hard partons of the colliding nuclei are Lorentz contracted to a region of order $2R_A/\gamma_{\text{cm}} \ll 1$ fm. We consider the collision region as a point in the longitudinal direction and assume that the rapidity of the minijet coincides with the space-time rapidity of the formation point, $y = \eta = (1/2) \ln[(t+z)/(t-z)]$. The formation (proper) time we take to be the inverse of the saturation scale, $\tau_0 = 1/p_{\text{sat}}$. Thus the minijet matter forms along the hyperbola $t = \sqrt{z^2 + \tau_0^2}$ with initial longitudinal flow velocity $v_z(\tau_0) = z/t$.

The basic quantities for the minijet production in a nucleon-nucleon collision are $\sigma_{\text{jet}}(p_{\text{sat}}, \sqrt{s}, \Delta y, A)$ and $\sigma_{\text{jet}} \langle E_T \rangle(p_{\text{sat}}, \sqrt{s}, \Delta y, A)$, the minijet cross section and its first moment in transverse energy (momentum) for the rapidity interval Δy , both integrated in p_T from $p_T = p_{\text{sat}}$ to infinity [1,3,4]. The number of minijets or the transverse energy in Δy in a nucleus-nucleus collision is obtained by multiplying the corresponding cross section with the nucleon-nucleon luminosity (with an extra factor 2 for the number of minijets) which for a central collision is $T_{AB}(0)$, the overlap function of transverse densities for the colliding nuclei: $T_{AB}(\mathbf{b}) = \int d^2\mathbf{s} T_A(|\mathbf{b} - \mathbf{s}|) T_B(s) = T_{AB}(b)$, $T_A(\mathbf{s}) = \int_{-\infty}^{+\infty} dz \rho_A(z, \mathbf{s}) = T_A(s)$, where \mathbf{b} is the impact parameter and \mathbf{s} the transverse coordinate.

Average densities are obtained by dividing with the volume $\Delta V = \Delta z A_T = \tau_0 \Delta y \pi R_A^2$. This procedure is easily generalized to local density in the transverse plane of the collision. The nucleon-nucleon luminosity for a transverse area element $d^2\mathbf{s}$ is $T_A(|\mathbf{b} - \mathbf{s}|) T_B(s)$ and the volume element $dV = dz d^2s = \tau \Delta y d^2s$ leading to [5]

$$n_{\text{pQCD}}(\tau_0, \mathbf{s}) = \frac{dN}{\tau_0 dy d^2s} = \frac{1}{\tau_0 \Delta y} 2T_A(|\mathbf{b} - \mathbf{s}|) T_B(s) \sigma_{\text{jet}},$$

and

$$\epsilon_{\text{pQCD}}(\tau_0, \mathbf{s}) = \frac{dE_T}{\tau_0 dy d^2s} = \frac{1}{\tau_0 \Delta y} T_A(|\mathbf{b} - \mathbf{s}|) T_B(s) \sigma_{\text{jet}} \langle E_T \rangle.$$

We next make a bold assumption of fast thermalization: we assume that the thermalization time scale is the same as that of production and for simplicity we take the system to be thermal right at the formation time τ_0 . Two simple arguments can be given in favour of this assumption. First, if we calculate the temperature either from $\epsilon(\tau_0)$ or $n(\tau_0)$, the result is very closely the same. This means that for thermalization only collisions causing energy and momentum transfer are needed, number changing reactions are not essential. Second, the time scale τ_0 is associated with the saturation scale and the formation time of more energetic (mini)jets could be shorter so that some secondary interactions take place already before the overall formation time.

In Figure 1 the transverse profile of the initial energy distribution is shown for a gold-on-gold collision at RHIC (dashed line) and lead-on-lead collision at LHC energy (solid

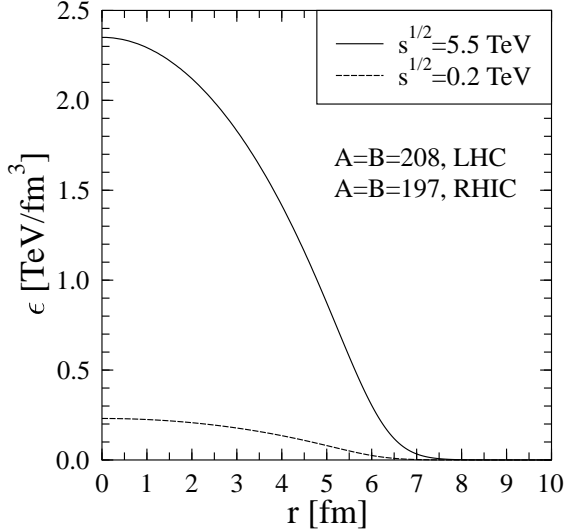


Figure 1. Transverse dependence of the initial energy distribution for a gold-on-gold collision at RHIC (dashed line) and lead-on-lead collision at LHC energy (solid line). The average value of the saturation scale is $p_{\text{sat}} = 1.16$ GeV at RHIC and 2.03 GeV at LHC with formation times 0.170 and 0.100 fm/c, respectively.

line). We comment on the values of multiplicity and transverse energy of initial minijets when discussing later the results on final hadron spectra.

3. HYDRODYNAMICS OF EXPANSION

We will assume isentropic expansion. Studies of viscous effects indicate that the entropy production during expansion does not produce significant effects [6]. The longitudinal flow is taken to be boost invariant and to scale at central rapidity. Then $v_z = z/t$ or equivalently $y = \eta$ and the energy density and transverse flow velocity are of form $\epsilon = \epsilon(\tau, r)$ and $v_T = v_T(\tau, r)$ [7]. With cylindrical symmetry the equations reduce to 1+1-dimensional form and finding out the solutions numerically is straightforward.

To close the set of hydrodynamical equations the equation of state (EoS) is needed. We have assumed an ideal QGP at high temperatures and a hadron gas including all hadrons and hadron resonances up to the mass 2 GeV. Repulsion of hadrons is described by mean field with $K = 450$ MeV and to induce a phase transition a bag constant is included in the EoS. Calculations presented here are performed with the bag constant $B^{1/4} = 235$ MeV leading to value $T_c = 165$ MeV for the phase transition temperature [8,9].

Finally, to turn the hydrodynamic quantities, the transverse velocity $v_T(\tau, r)$ and the local temperature $T(\tau, r)$ to observable quantities, the thermal motion, characterized by T , must be folded with the flow motion v_T . This is done using the Cooper and Fry prescription [2]. Final particles are assumed to decouple from the thermal phase at a given density ϵ_{dec} or equivalently in the zero baryon number case at temperature T_{dec} . The condition $T(\tau, r) = T_{\text{dec}}$ defines a hypersurface σ^μ and the particle spectra are obtained as the net particle number flow through this surface. For the boost-invariant cylindrically symmetric case the integration can be reduced to one-dimensional integrals:

$$\begin{aligned} \frac{dN}{dy dp_T^2} &= \frac{g}{2\pi} \sum_{n=1}^{\infty} (\pm 1)^{n+1} \int_{\sigma} r \tau \left[-p_T I_1(n\gamma_r v_r \frac{p_T}{T}) K_0(n\gamma_r \frac{m_T}{T}) d\tau \right. \\ &\quad \left. + m_T I_0(n\gamma_r v_r \frac{p_T}{T}) K_1(n\gamma_r \frac{m_T}{T}) dr \right]. \end{aligned} \quad (1)$$

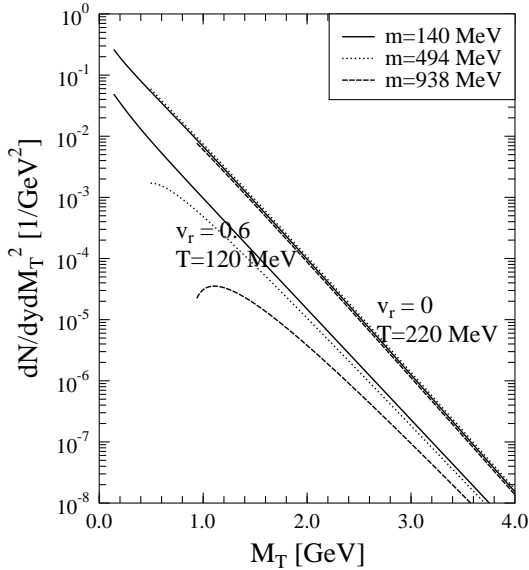


Figure 2. Thermal spectra exhibit transverse mass scaling when $v_r = 0$. For non-zero transverse velocity ($v_r = 0.6$) transverse spectra of particles depend not only on M_T but also on M . Temperatures are arbitrary but so chosen that all spectra have approximately the same slope at large M_T .

Without transverse flow the first term is missing and the second term depends only on the transverse mass $M_T = \sqrt{p_T^2 + M^2}$ and temperature T . Equation 1 shows explicitly the breaking of M_T scaling through the p_T dependent terms when $v_T \neq 0$. This is shown in Figure 2 where pion, kaon and proton spectra are shown for $v_T = 0$ and $v_T = 0.6$. The temperatures, $T = 220$ MeV when $v_T = 0$ and $T = 120$ MeV when $v_T = 0.6$, are so chosen that the slopes at large m_T are similar. For $v_T = 0$ the mass shows up only in the starting point of the spectrum. (There is a difference between bosons and fermions from the alternating sign for the latter in the summation.) For non-zero transverse flow the spectra deviate from the scaling behaviour mainly in the region $p_T \lesssim M$. When p_T is clearly bigger than m , the spectra become similar since $p_T \sim M_T$. In nuclear collisions the spectra get contributions over a range of transverse velocities, but the general features remain the same as in Figure 2 for $v_T = 0.6$.

The buildup of transverse flow is one manifestation of the collective behaviour of a dense system. The estimates, using as input the Lorentz contracted nuclear geometry and the observed multiplicities, give quite high particle densities. With such densities it would be difficult to understand the dynamics of the produced matter if no collective effects are observed since this would indicate that the final state particles interact very weakly.

In any approach based on dominance of hard processes in the initial particle production the predicted transverse energy will be consistent with observations only if the system behaves collectively: the initially produced transverse energy is much higher than the observed one as discussed in detail in Section 4. In the fast longitudinal hydrodynamic expansion a large fraction of this energy is transferred into the longitudinal motion which should show up in the broadening of rapidity spectra from their initial shape. In the present boost invariant calculation only the energy loss in the central rapidity region can be calculated.

4. RESULTS AND COMPARISON WITH EXPERIMENT

The calculations are performed for central collisions when the produced matter distributions are cylindrically symmetric. Since the RHIC data is given for a 6 % centrality cut, we use in calculating the initial minijet production an effective mass number for nucleons fixed to equal the average number of participants for that centrality cut; for details see [5]. We assume a similar centrality cut in predictions for the LHC energies. To show the magnitude of the change from imposing the cut, we perform the calculations also with mass numbers $A = 197$ for gold at RHIC and $A = 208$ for lead at LHC.

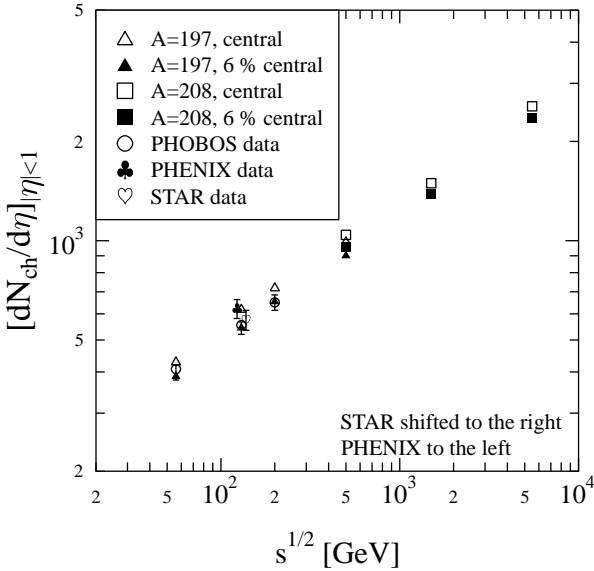


Figure 3. Charged particle multiplicity as function of collision energy [5]. Calculations (triangles and squares) are for the full (open) and effective (filled) mass number determined from centrality.

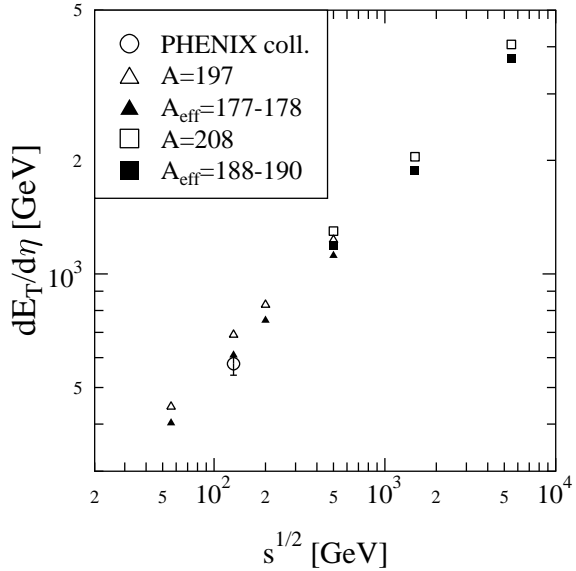


Figure 4. As in the left panel but for total transverse energy [5]. The initial transverse energy at $\sqrt{s} = 130$ GeV is also displayed.

I will begin by presenting results on p_T -integrated quantities and finish by discussing the transverse spectra. All results are for mid-rapidity since the minijet calculation is performed at $y = 0$ and boost invariance is assumed in the hydrodynamic calculation.

Figures 3 and 4 display the dependence of the charged particle multiplicity and the total transverse energy on the collision energy. The charged particle multiplicity has been measured by PHOBOS Collaboration [11] at three different collision energies, $\sqrt{s_{NN}} = 56, 130$ and 200 GeV. There are some uncertainties in the normalization of the minijet calculation. E.g., the saturation condition for the cut-off momentum in minijet production, p_{sat} , could contain extra factors of order 1 but the simplest choice with no such factors is taken. However, once the normalization is fixed, the energy dependence is strongly constrained. There are still uncertainties common to all hard scattering approaches like those coming from higher order contributions. For the minijet calculation used here for

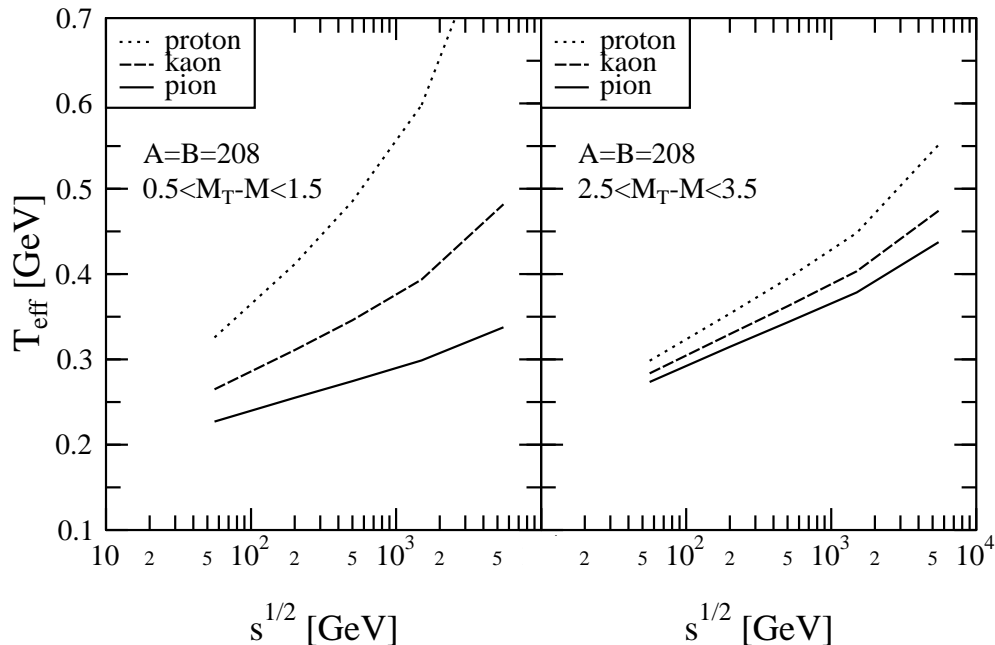


Figure 5. Effective temperatures determined as inverse slopes of pion, kaon and proton spectra at the LHC energy $\sqrt{s} = 5500$ GeV for two different transverse mass intervals.

the initial conditions, the contribution from the NLO terms has been calculated for the transverse energy; for details see [1,10]. The agreement of calculated multiplicities with the PHOBOS data [11] is very good both in normalization and the energy dependence. The values measured at \sqrt{s} by PHENIX [12] and STAR [13] Collaborations are 5...10 % higher.

For transverse energy the value measured by PHENIX Collaboration at $\sqrt{s} = 130$ GeV [14], 578 GeV, is ~ 6 % smaller than the calculated value 614 GeV. This should be compared with the initial value ~ 1550 GeV, also depicted in Figure 4 showing an almost a factor of 3 reduction of $dE_T/d\eta$ due to the expansion. On the other hand, as pointed out above, the multiplicity measured by PHENIX [12] is somewhat above our calculated value. This is an indication that, even though the energy in the transverse degrees of freedom is reduced by a large factor during the expansion, our calculated spectra, to be discussed below, are still slightly shallower than the measured ones.

Figure 5 shows the results on effective temperatures T_{eff} , the inverse slope of the spectrum, for pions, kaons and protons. When the flow destroys the scaling in transverse mass, the slope of the distributions becomes sensitive on the mass of the particle and changes rapidly with M_T (or p_T) especially in the region $M_T \lesssim (2 \dots 3)M$ as was seen in Figure 2. For this reason T_{eff} is displayed for two different transverse mass intervals, $0.5 < M_T - M < 1.5$ and $2.5 < M_T - M < 3.5$, in the left and the right panels of the Figure, respectively. At the smaller transverse mass values the mass dependence of slopes is very strong.

At $\sqrt{s} = 130$ GeV, the STAR collaboration has data on inverse slopes at small trans-

verse mass, $0.05 \text{ GeV} < M_T - M < 0.45 \text{ GeV}$ [15]. These are displayed in Table 1 (in MeV units) with inverse slopes from the calculated spectra at $M_T - M = 0.3 \text{ GeV}$. One observes that the calculated values are slightly larger than the measured ones but the ratios of the measured or the calculated slopes for different particles are quite similar.

T_{eff}	Pion	Kaon	Proton
Measured	190	300	565
Ratios	1	1.58	2.97
Calculated	238	387	652
Ratios	1	1.63	2.74

Table 1

Inverse slopes, T_{eff} in MeV, of pion, kaon and proton spectra measured at RHIC at $\sqrt{s} = 130 \text{ GeV}$ [15] and compared with calculated values.

Figure 6 shows the calculated average transverse momentum for different particles. In addition to the STAR measurement [15] at RHIC, also the NA49 [16] and the UA1 [17] data points are depicted. Comparable to the STAR measurement is $\langle p_T \rangle_{\text{all}} = \sqrt{\langle p_T^2 \rangle}$ calculated for all particles and shown as the filled circle. The calculated value is somewhat too large as were also the inverse slopes. Comparison of the STAR measurement with the UA1 point shows clearly a strong nuclear effect and the increase from the NA49 measurement indicates that the effect grows with energy. In a thermal model with expansion, this behaviour is understood in terms of increasing collective flow as the initial densities grow with the collision energy.

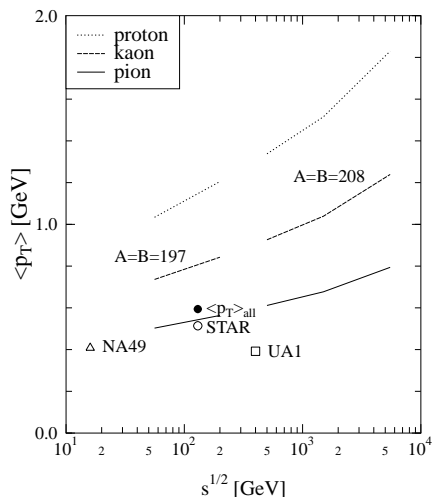


Figure 6. The average p_T of pions, kaons and nucleons as a function of collision energy. In addition to the STAR [15] data point, also NA49 [16] and UA1 [17] results are shown.

Transverse spectra of pions, kaons and protons are shown in Figure 7 at $\sqrt{s} = 200 \text{ GeV}$ and 5500 GeV . The breaking of M_T scaling is clearly seen. It should be emphasized that the normalization of kaons and protons relative to pions depends strongly on the decoupling temperature which is here assumed to be the same for all particles, $T_{\text{dec}} \simeq 120 \text{ MeV}$. It is more likely that the number of kaons [18] and protons freezes out earlier than at the kinetic freeze-out. This would increase their normalization relative to pions but the

shape of the spectrum could change less since the elastic collisions could still take place. In calculating the strange particle spectra, full chemical equilibrium is used at freeze-out. At lower energies strangeness is known to deviate from the equilibrium values [19]. We have also ignored the non-zero net baryon number which affects the normalization of (anti)proton spectrum at RHIC but less at LHC.

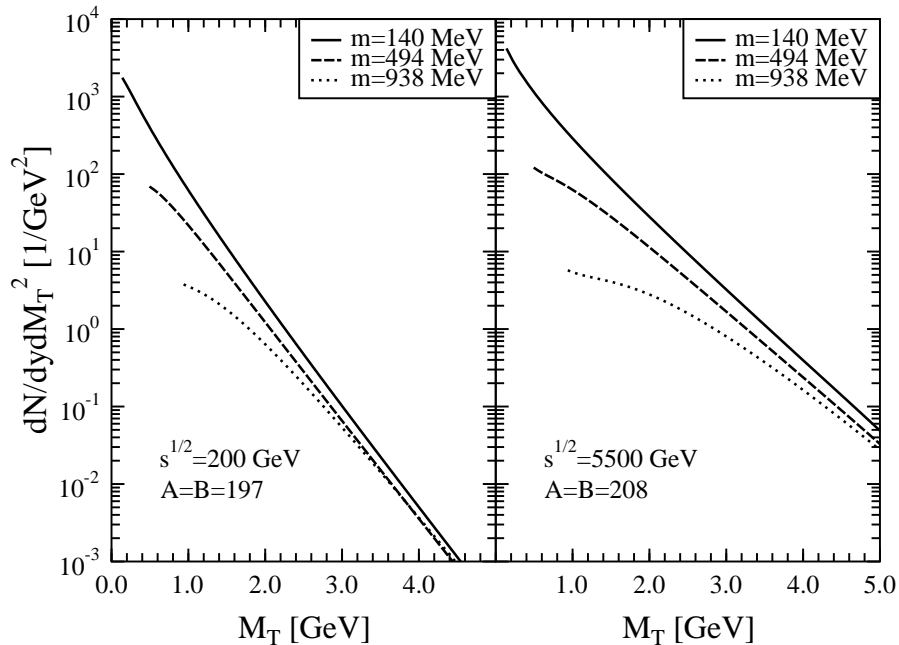


Figure 7. Transverse mass distributions of pions, kaons and protons. In calculating the proton spectrum, zero baryon chemical potential is used. The spectra contain also the particles from decays of resonances up to $\Sigma(1385)$.

In Figure 8 the calculated transverse momentum spectrum of negative particles at $\sqrt{s} = 130$ GeV is compared with the spectrum measured by the STAR Collaboration [13]. There is an indication of difference in shape at small transverse momenta. In the calculation the turning down of the spectrum comes from the Jacobian, p_T/M_T . At large values of transverse momentum the calculated spectrum is somewhat above the measured one. This was already seen when comparing the values of inverse slopes and average transverse momenta. In terms of the total reduction of energy in the transverse degrees of freedom by almost a factor of three this is a small effect and we have not tried to fine tune the calculation.

5. CONCLUSIONS

We have combined a minijet calculation of initial particle production at collider energies with a hydrodynamic treatment for describing the expansion of the produced matter. This allows us to predict particle spectra, particle multiplicities and the transverse energy of

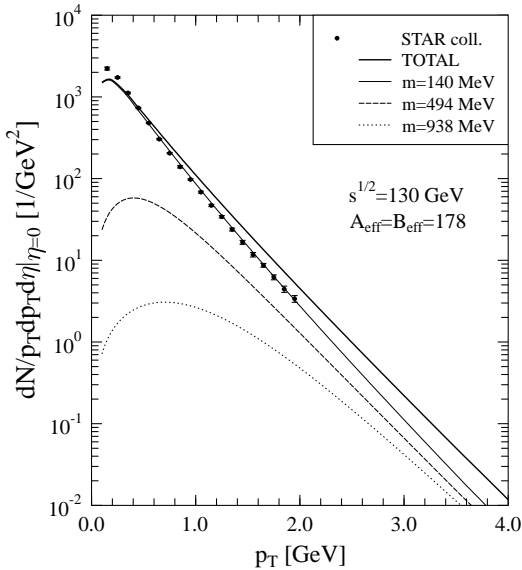


Figure 8. Transverse momentum spectrum of negative particles. The data points, presented as filled circles are from STAR Collaboration [15]. The calculated spectrum (thick solid line) contains the contributions of π^- , K^- and antiproton, shown also separately.

final particles as a function of the mass number of the colliding nuclei and the collision energy.

The prediction from the minijet calculation of the initial particle production which is most robust against details of the treatment of the expansion is the multiplicity density, $dN/d\eta$ (or dN/dy), since this assumes only an approximate conservation of entropy. Since, as was shown in Section 2, the energy and the number density of the initially produced minijets correspond to the same thermal state, the number changing reactions are not important for thermalization and the entropy production after initial minijet production can be expected to be small. The calculations agree very well with the PHOBOS data at each of the three RHIC energies. At 130 GeV the PHENIX and STAR results are above the calculated value but they are also higher than the PHOBOS result.

The initial energy per produced parton is quite large. E.g. the calculated average transverse momentum of initial minijets is $\langle p_T \rangle_i \simeq 1.47$ GeV at the RHIC energy $\sqrt{s} = 130$ GeV and 3.2 GeV at the full LHC energy $\sqrt{s} = 5500$ GeV. After the expansion stage the calculated value at $\sqrt{s} = 130$ GeV is $\langle p_T \rangle_f = 0.594$ GeV to be compared with the measured value 0.514 GeV. This slight discrepancy in the predicted and measured transverse momentum quantities shows up also in the inverse slopes or effective temperatures determined from the spectra. E.g., the calculated values of T_{eff} at $M_T = 0.3$ GeV are 20...25 % larger at $\sqrt{s} = 130$ GeV than the measured ones. However, the predicted mass dependence comes out qualitatively right. The thermal model with collective transverse flow predicts a strong dependence of the slope both on mass and transverse mass in the transverse mass range $M_T - M \lesssim 2M$.

The results from the minijet calculation with saturation assumption combined with the hydrodynamic description of the expansion of final matter look quite promising when compared with the first measurements at RHIC. This description of nuclear collisions provides a well constrained framework for the study of other signals, like the photon and lepton pair emission or the evolution of strangeness and the heavier flavours during the final dense state.

Acknowledgements: I should like to thank my collaborators, K.J. Eskola, S.S. Räsänen and K. Tuominen for discussions and assistance and the Academy of Finland for financial support.

REFERENCES

1. K.J. Eskola, this volume.
2. F. Cooper and G. Frye, Phys. Rev. D **10**, 186 (1974).
3. K. J. Eskola, K. Kajantie, P. V. Ruuskanen and K. Tuominen, Nucl. Phys. B **570** (2000) 379, [arXiv:hep-ph/9909456].
4. K. J. Eskola, K. Kajantie and J. Lindfors, Nucl. Phys. B **323** (1989) 37.
5. K. J. Eskola, P. V. Ruuskanen, S. S. Räsänen and K. Tuominen, Nucl. Phys. A, in press, arXiv:hep-ph/0104010.
6. M. C. Chu, Phys. Rev. D **34** (1986) 2764.
7. J. D. Bjorken, Phys. Rev. D **27**, 140 (1983).
8. P. Huovinen, P. V. Ruuskanen and J. Sollfrank, Nucl. Phys. A **650** (1999) 227 [nucl-th/9807076].
9. J. Sollfrank, P. Huovinen, M. Kataja, P. V. Ruuskanen, M. Prakash and R. Venugopalan, Phys. Rev. C **55** (1997) 392 [nucl-th/9607029].
10. K. J. Eskola and K. Tuominen, Phys. Lett. B **489** (2000) 329 [hep-ph/0002008]; K. J. Eskola and K. Tuominen, Phys. Rev. D **63** (2001) 114006 [arXiv:hep-ph/0010319].
11. B. B. Back *et al.* [PHOBOS Collaboration], Phys. Rev. Lett. **85** (2000) 3100 [arXiv:hep-ex/0007036]; B. B. Back *et al.* [PHOBOS Collaboration], arXiv:nucl-ex/0108009.
12. K. Adcox, *et al.* [PHENIX Collaboration], Phys.Rev.Lett. **86** (2001) 3500-3505 [nucl-ex/0012008].
13. C. Adler *et al.* [STAR Collaboration], Phys. Rev. Lett. **87** (2001) 112303 [nucl-ex/0106004].
14. K. Adcox, *et al.* [PHENIX Collaboration], Phys.Rev.Lett. **87** (2001) 052301 [nucl-ex/0104015]
15. J. Harris for STAR Collaboration, Invited talk at Quark Matter 2001.
16. H. Appelshäuser *et al.* [NA49 Collaboration], Phys. Rev. Letters, **82** (1999) 2471.
17. C. Albajar *et al.*, Nucl. Phys. B **355** (1990) 261.
18. K. Kajantie, M. Kataja and P. V. Ruuskanen, Phys. Lett. B **179** (1986) 153.
19. J. Sollfrank, P. Huovinen, M. Kataja, P. V. Ruuskanen, M. Prakash and R. Venugopalan, Phys. Rev. C **55** (1997) 392 [arXiv:nucl-th/9607029].